BJRS
BRAZILIAN JOURNAL OF RADIATION SCIENCES

doi.org/10.15392/2319-0612.2025.2777
2025, 13(1) | 01-34 | e2777
Submitted: 2024-09-18
Accepted: 2024-11-13

Exploring the radiation shielding efficiency of low-impact Portland cement pastes made with barium sulfate, silica fume and fly ash

Pires[a*], M. M.; Souza, E. G.[b]; Nascimento, C. D.[b]; Sobreira, L. C[a]; Maia, I.Z. [a]; Trombini, H.[c]; Santos, R. R.[d]; Ribeiro, F. R. C.[e]; Mancio, M.[a]; Kazmierczak, C. S.[a]; Kulakowski, M. P.[a]

[a] Programa de Pós-Graduação em Engenharia Civil, PPGEC, Universidade do Vale do Rio dos Sinos, UNISINOS, São Leopoldo, RS, Brasil.
[b] Mestrado em Engenharia Eletrônica e Computação, Universidade Católica de Pelotas, UCPel, Pelotas, RS, Brasil.
[c] Departamento de Ciências Sociais Exatas e Aplicadas, Universidade Federal de Ciências da Saúde de Porto Alegre, UFCSPA, Porto Alegre, RS, Brasil.
[d] Hospital de Clínicas de Porto Alegre, HCPA, Porto Alegre, RS, Brasil.
[e] Programa de Pós-Graduação em Engenharia Civil, PPGCI, Universidade Federal do Rio Grande do Sul, UFRGS, Porto Alegre, RS, Brasil.

*Correspondence: maikonnpires@edu.unisinos.br

Abstract: The scope of this work is the development of new composites with low environmental impact to act as radiological shielding in hospital environments. For this purpose, the radioprotection properties of cement pastes containing 20% $BaSO_4$, in addition to 10% fly ash and silica fume as SCM's were investigated. The samples were characterized by consistency, apparent density and mechanical strength at 7 and 28 days of age. In addition, transmission measurements were performed for different sample thicknesses using a photon beam from a linear accelerator operating at 6 and 10 MV in a radiotherapy room. The barium pastes showed a reduction in sample thickness of approximately 10% compared to the reference paste (without barium) at the highest voltage analyzed to attenuate 90% of the incident radiation (according to current legislation). Among the SCM's, silica fume stood out as the most suitable substitute when combined with barium in Portland cement matrices. Finally, the apparent density of the samples appears to be decisive for the performance of new materials in terms of radiological shielding.

Keywords: Cementitious pastes, Barium sulfate, Protection barriers, Ionizing radiation, Radiotherapy.

doi.org/10.15392/2319-0612.2025.2777
2025, 13(1) | 01-34 | e2777
Submitted: 2024-09-18
Accepted: 2024-11-13

Explorando a eficiência da proteção contra radiação de pastas de cimento Portland de menor impacto ambiental elaboradas com sulfato de bário, sílica ativa e cinza volante

Resumo: O escopo deste trabalho está no desenvolvimento de novos compósitos de baixo impacto ambiental para atuarem na blindagem radiológica em ambientes hospitalares. Para tanto, foram investigadas as propriedades de radioproteção de pastas cimentícias contendo 20% de $BaSO_4$, além de 10% de cinza volante e sílica ativa como MCS. As amostras foram caracterizadas através da consistência, densidade aparente e resistência mecânica aos 7 e 28 dias de idade. Além disso, foram realizadas medidas de transmissão para diferentes espessuras de amostras utilizando um feixe de fótons de um acelerador linear operando a 6 e 10 MV em uma sala de radioterapia. As pastas de bário apresentaram redução na espessura da amostra de aproximadamente 10% em relação a pasta referência (sem bário) na maior voltagem analisada para atenuar 90% da radiação incidente (conforme legislação vigente). Dentre os MCS, a sílica ativa se destacou como o substituto mais adequado quando combinada ao bário nas matrizes de cimento Portland. Por fim, a densidade aparente das amostras parece ser decisiva para no desempenho de novos materiais frente a blindagem radiológica.

Palavras-chave: Pastas cimentícias, Sulfato de bário, Barreiras de proteção, Radiação ionizante, Radioterapia.

1. INTRODUCTION

With the development of science and technology, ionizing radiation in medicine has become increasingly important, especially in radiotherapy, for treating most malignant cancers [1-2]. It is estimated that half of patients diagnosed with cancer undergo radiotherapy at some point during their treatment after the disease is diagnosed, from curative treatment to symptom relief [3-5]. With the expansion of imaging techniques, radiotherapy has become widespread, used alone or in conjunction with other oncological therapies [6].

In order to combat cancer, radiotherapy uses the principle of ionizing radiation, defined as the energy capable of extracting electrons from the orbit of an atom [7-9]. It is known that this type of radiation can cause consequences for patients, such as cell death, DNA changes, or even carcinogenesis [10]. However, the damage caused by ionizing radiation to human tissue was only noticed after two decades of use following the discovery of X-rays by Röentgen in 1895 [11]. Since then, the Röentgen Society has been one of the pioneers in publishing recommendations on the radiological protection of users [12].

To comply with national and international standards, protective barriers (shielding) must be designed to guarantee the health of health professionals exposed inside and outside the work environment, ensuring that they are not exposed to doses that exceed the permitted limit [13]. Currently, radiotherapy rooms are isolated with a reinforced concrete structure that is expensive to build. According to Agrawal *et al.* [14], to build radiological protection structures in diagnostic and computed tomography rooms, walls approximately 6" thick (15.0 cm) are required, as they use much lower tensions than radioprotection rooms, which have thicknesses exceeding 200.0 centimeters, which is why they areet al also called bunkers [15].

With a view to optimizing the construction process of radiotherapy environments, several studies have investigated ways of producing cementitious materials with high

protection capacity, reduced thickness, and high density. Materials such as iron-rich red mud, concrete based on serpentine and hematite, and cementitious matrices with steel fiber have already been investigated and have shown good attenuation capacity; however, they did not outperform conventional concrete [16–19]. Barium sulfate ($BaSO_4$ or barite) is one of the few non-metallic minerals with a specific mass high enough to attenuate electromagnetic radiation. Furthermore, it is affordable and widely available [20–22]. For this reason, it has been evaluated for use as a protective barrier through computer simulations [23–26] and experimental studies [27–32].

Furthermore, barite has a good relationship with several composites to obtain new materials, proving to be an excellent alternative to lead. This heavy metal is highly toxic and causes environmental problems regarding its disposal [27, 33]. In producing cementitious composites, whether pastes, mortars, or concrete, Portland cement is replaced by supplementary cementitious materials (SCM's) as additional components to improve properties in the fresh and hardened state. This reduces carbon dioxide (CO_2) emissions in cement production, and millions of tons of industrial byproducts are no longer discarded into nature. Among the residues that can be used against ionizing radiation are silica fume and fly ash. Silica fume tends to fill the voids between cement particles, densifying the binder paste matrix. Fly ash reduces the heat of hydration of cement and improves the workability of concrete due to its physical characteristics [34-36]. Previous studies have evaluated the shielding capacity of Portland cement matrices incorporated with barium sulfate, with concrete being the most common matrix type, followed by Portland mortar matrices [21, 30, 31, 37-43]. However, the isolated effects of Portland cement pastes incorporated with barite and SCM's for shielding ionizing radiation in hospital environments have not been evaluated.

Given the context presented, the present study proposed the preparation of Portland cement pastes with the addition of barium sulfate and SCM's (fly ash and silica fume), to investigate the properties of these matrices in the shielding of photon beams from a linear

accelerator in a radiotherapy room. For this purpose, the properties of the pastes were evaluated in the fresh and hardened states after 7 and 28 days. As control factors, there are the unit compositions of the pastes, water/cement ratio (w/c), and the percentage of additive, as well as response factors; there is the slump, the axial compressive strength, the apparent density, and the attenuation coefficient against radiological shielding.

2. MATERIALS

The binder adopted to prepare the barium pastes was white Portland cement manufactured by the company Secil (Pataias Gare/Pataias/Portugal). Barium pastes are so called because they use natural barium sulfate (or barite) in their composition, a mineral of inorganic constitution, chemically inert, extracted from deposits and arranged in different particle sizes. It has the chemical formula $BaSO_4$, a density of 4.21 g/cm³ and a purity of 98.24%, coming from Neon (São Paulo/São Paulo/Brazil).

As SCM's, fly ash and silica fume partially replaced white cement. The first residue was obtained from burning mineral coal to produce electrical energy, provided by the Presidente Médici Thermoelectric Plant (Candiota/Rio Grande do Sul/Brazil). The company Diprotec (Curitiba/Paraná/Brazil) supplied the second material, a by-product produced during the metal silicon and ferrosilicon smelting process. PowerFlow 1180 was used as a chemical admixture, a high- performance superplasticizer supplied by Concreto Schumann (Pelotas/Rio Grande do Sul/Brazil).

2.1. Physical Characterization

The results obtained for the physical characterization of the materials are presented in Table 1. Starting with laser diffraction granulometry, a widely adopted technique for evaluating materials with small granulometry, was chosen to obtain the average particle sizes. This technique was performed using the Microtrac particle size analyzer, model

S3500. The solvent used was isopropyl alcohol to analyze the white cement and hexametaphosphate to check the other materials.

Table 1: Physical characterization of materials.

PHYSICAL PROPERTIES	WHITE CEMENT	FLY ASH	SILICA FUME	BARIUM SULFATE
D_{10} (μm)	4.25	7.34	1.73	0.51
D_{50} (μm)	9.73	34.33	6.35	0.87
D_{90} (μm)	22.95	69.58	14.66	1.98
SSA (m^2/g)	1.50	0.74	17.77	3.15
Especific mass (g/cm^3)	2.96	2.06	2.21	4.21

The particles' specific surface area (SSA) was determined using the BET method from the quantification of the volume of nitrogen in the layer adsorbed on the material's surface. This analysis considers factors such as the shape and texture of the particle on the surface of the grain [44]. This test was chosen because nitrogen can consider aspects such as porosity, roughness and cracks in the result, therefore, it presents a higher value than those determined by Blaine and has been widely used [45].

Before carrying out the test using the BET method, the samples were subjected to pre-treatment to desorb gases present in the material to mitigate interference in the readings, as described by Mantellato, Palacios and Flatt [46]. Thus, following the authors' procedure, the white cement was subjected to gas desorption at 40ºC for 16 hours in a nitrogen atmosphere. On the other hand, the rest of the materials underwent the same process, however, at temperatures around 200ºC for 1 hour. This temperature difference arises from the possible dehydration of materials such as anhydrous cement at high temperatures. The equipment used to carry out the test is Micromeritics, model Tristar Plus II.

The specific mass of the materials was determined using the helium gas pycnometer technique, which, using pressure, penetrates gas into the sample's pores. At the end of the test, the pressure value collected is correlated with the pore volume of the respective sample. The specific mass of the material under analysis is determined from the actual volume and mass of

the sample. The samples were less than 15.0 cm³ and were free of impurities and moisture. This technique was performed using Micromeritics equipment, model AccuPyc II 1340.

2.2. Chemical Characterization

X-ray fluorescence (XRF) is a technique that allows a qualitative and quantitative analysis of the chemical elements that make up the sample. It is a qualitative analysis, as it identifies the chemical elements present in the sample and qualitative, as it presents the proportion in which each element is found. This study was conducted on the Shimadzu X-ray fluorescence spectrometer, model EDX-720. Previously, the samples were dried in an oven and then compacted to form tablets.

Table 2 shows the results of the qualitative analysis chemical of barium sulfate and Table 3, the results of the quantitative analysis of white cement, fly ash and silica fume.

Table 2: Qualitative chemical characterization of barium sulfate.

MAJORITY ELEMENTS (> 50%)	SMALLEST AMOUNT (5% < X < 50%)	TRACE ELEMENTS (< 5%)
Ba	S	V, P, Sr, Ca

Table 3: Quantitative chemical characterization of white cement, fly ash and silica fume in percentage.

MATERIALS	SiO_2	Al_2O_3	Fe_2O_3	CaO	Na_2O	MgO	P_2O_5	SO_3	K_2O	TiO_2	Cr_2O_3	MnO	SrO	ZnO	PF
WHITE CEMENT	16.25	1.91	0.18	67.47	1.19	0.54	0.10	1.34	0.31	0.10	0.01	0.02	0.02	ND	10.56
FLY ASH	61.23	20.24	9.69	2.59	0.09	1.54	0.20	0.87	1.91	1.11	ND	ND	ND	ND	0.53
SILICA FUME	91.42	1.96	0.13	0.53	ND	ND	ND	1.34	2.72	ND	ND	ND	ND	ND	1.90

3. METHODS

3.1. Paste Dosage and Sample Preparation

Four different mixtures of Portland cement pastes were proposed to enable a comparative analysis of the performance of different compositions in terms of shielding against ionizing radiation. The samples were called T.REF (reference paste without the

addition of barium and SCM's), T.BA (with the addition of barium), T.BA.FA (adding barium and partial replacement of Portland cement with fly ash) and T.BA.SF (with the addition of barium and partial replacement of Portland cement with silica fume), as indicated in Table 4.

Table 4: Cement paste compositions in percentage.

MATERIAL	T.REF (%)	T.BA (%)	T.BA.FA (%)	T.BA.SF (%)
White cement	100	80	70	70
Barium sulfate	-	20	20	20
Fly ash	-	-	10	-
Silica fume	-	-	-	10
Water/solids ratio	25	25	25	25
Superplasticizer	0.55	0.55	0.55	0.55

Three of the proposed compositions contain barium sulfate, which is why they are called barium pastes. The percentage of barium used in these three pastes was constant (20%). The compositions T.BA.FA and T.BA.SF differ from T.REF by replacing 10% white cement with pozzolanic material (silica fume or fly ash). The ratio of water to solid materials remained constant (w/s = 0.25), as did the percentage of superplasticizer additive (0.55%) about the total mass of the binder.

The pastes evaluated were produced in an air-conditioned room with a controlled temperature of 21±2°C and relative humidity of 60±10%. The first mixing process was dry using a Cortag brand electric mortar mixer with 1600 watts of power. A minimum time of 10 minutes was stipulated to carry out this process. At this mixing stage, approximately 440 rpm was adopted. After dry mixing, the mixing process began with adding water and superplasticizer admixture. The average time required for the traces to reach homogenization was 12 minutes, and the equipment rotation reached 660 rpm. The test specimens were molded according to NBR 5738 [47].

For mechanical tests, 80 cylindrical samples (31.0 mm in diameter and 62.0 mm in height) were moulded to determine the apparent density and resistance to axial compression at 7 and 28 days of age. The density adopted was manual by NBR 5738 [47]. The specimens

remained at room temperature for the first 24 hours and, after this period, they were demolded and went through the curing process in a humid chamber with relative humidity ≥ 95%. In Table 5, it is possible to check the number of moulded specimens for each trait depending on the sample type and age at failure.

Table 5: Number of cylindrical specimens for the axial compressive strength test.

PASTE	7 DAYS	28 DAYS	TOTAL
T.REF	10	10	20
T.BA	10	10	20
T.BA.FA	10	10	20
T.BA.SF	10	10	20
TOTAL	40	40	80

To expose the pastes to radiation, prismatic samples were moulded for each line with a section of 12.0 x 12.0 cm and varying thicknesses (1.0, 3.0 and 6.0 cm) in wood covered with plastic foil. Table 6 illustrates the number of units for each proposed thickness. The densification adopted was also manual by NBR 5738 [47]. The specimens remained at room temperature for the first 48 hours and, after this period, they were demolded and went through the curing process in a humid chamber with relative humidity ≥ 95%.

Table 6: Number of prismatic specimens for exposure to ionizing radiation.

DIMENSION (cm)	THICKNESS (cm)	QUANTITY (units)	TOTAL THICKNESS (cm)
12.0 x 12.0	1.0	1.0	1.0
12.0 x 12.0	3.0	1.0	3.0
12.0 x 12.0	6.0	5.0	30.0
TOTAL		7.0	34.0

3.2. Properties of Fresh Pastes

The truncated cone mini-slump method was adopted to determine the consistency of the pastes, as recommended by Kantro [48]. The paste was inserted into the mini-cone on a glass plate with graph paper. The cone was then removed perpendicularly to the glass plate, and the spread was measured at the end of the process in two orthogonal axes (X and Y), as

illustrated in Figure 1. The consistency of the pastes was considered a response factor, and the w/s and percentage ratio of the superplasticizer as a controlling factor.

Figure 1: Kantro mini-cone test: a) beginning of the test, b) scattering measured on the X-axis and, c) scattering measured on the Y-axis.

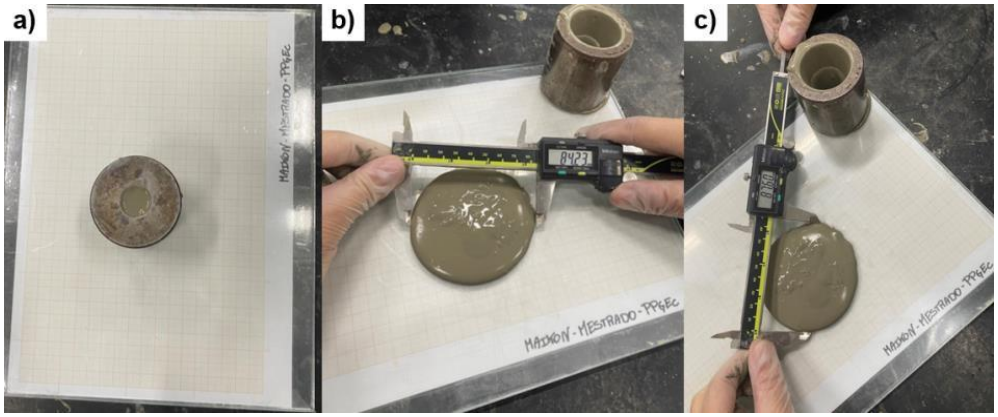

3.3. Paste Properties in the Hardened State

To carry out the test that determines the resistance to axial compression, NBR 7215 [49]. The press used is from the Emic-Instron brand, model PC 100C - Class II, with a capacity of 100 tons and a breaking speed of 100 N/s.

3.4. Attenuating Properties of Photon Beams

To analyze the shielding capacity of the four types of cement pastes, prismatic specimens with a section of 12.0 x 12.0 cm and variable thicknesses (t) (1.0, 3.0 and 6.0 cm) were moulded. The moulds were arranged sequentially, one after the other, forming a layer up to 34.0 cm thick. The samples were positioned in the isocenter of the Varian linear electron accelerator, model True Beam, at a source-isocenter distance of 100.0 cm with a field size of 10.0 x 10.0 cm on the surface. Thus, the distance from the source to the specimens (SSD) for each sample can be calculated by the following expression:

$$SSD = 100.0 - t \quad (1)$$

Then, all samples were exposed to photon beam radiation with nominal voltages of 6 MV and 10 MV, with a dose rate of 600 cGy/min. To measure the radiation, a PTW

electrometer, model TN30013, with a nominal voltage of -300 V was used, which was positioned behind the samples in order to collect the radiation transmitted by the test specimens, following the methodology proposed by Pires *et al.* [28] and Pires *et al.* [29]. The arrangement of the samples is illustrated in Figure 2.

Figure 2: Top view of samples with different thicknesses being exposed to ionizing radiation in the linear electron accelerator. During the experiment, spacing between samples was not considered. The figure shows type "C" samples that refer to the T.BA.FA folder samples.

The values of semi-reductive and de-reductive layers must be referenced during the shielding calculation in the Final Safety Analysis Report. Therefore, the attenuation of the beam was evaluated for a de-reducing layer, corresponding to 90% of the original intensity. To verify this percentage for all samples, a decreasing exponential fit (not shown) was performed based on the experimental data obtained. The fit was performed using the equation $\boldsymbol{I = I_0\, e^{-kx}}$, where $\boldsymbol{I}$ represents the percentage of the desired initial intensity, $\boldsymbol{I_0}$ represents the maximum intensity obtained located at the maximum dose point (with 100% transmitted radiation), $\boldsymbol{x}$ represents the thickness of the cement pastes and, finally, $\boldsymbol{k}$ is the linear attenuation coefficient. The same equation can be used to determine the semi-reducing layer.

4. RESULTS

4.1. Properties of Fresh Pastes

Table 7 presents the results obtained for paste consistencies (medium spread). The most excellent spread was observed in the reference paste, but as other additions and substitutions were made to the mixtures, losses in the consistency of the matrices were observed. It can be seen that the paste that presented the lowest average spreading (T.BA) has barium sulfate added to its composition. This loss of consistency is approximately 21% when compared to T.REF paste. As demonstrated in the physical characterization of the materials, barite presented SSA 110% higher than Portland cement, which possibly justifies this reduction result. Furthermore, the ore also presented a higher specific mass and smaller particle size (smaller grain) when compared to the binder. Materials with smaller granular sizes (fine) tend to agglomerate and increase matrix water consumption [50-51]. Authors such as Zhang *et al.* [52], Wang, Zhang and Sun [53] and Mehdipour and Khayat [54] elucidate that in cement matrices, there may be filling water that runs through the voids in the sample and does not contribute to the consistency, as well as water may be present on the surface of the grains in addition to the porosity, providing workability to the cement paste.

Table 7: Orthogonal and average scatterings obtained with the Kantro mini-cone.

PASTE	X-AXIS SCATTERING (mm)	Y-AXIS SCATTERING (mm)	MEDIUM SPREAD (mm)
T.REF	120.56	121.15	120.86
T.BA	96.77	98.58	97.68
T.BA.FA	101.32	103.69	102.51
T.BA.SF	99.92	100.75	100.34

Therefore, the water in the T.BA paste was possibly sufficient for percolation in the sample but not enough to be accessible on the surface of the grains. This effect can be justified by the agglomeration of particles generated due to the high specific surface area,

reduced grain size of barite, and high density. Like the others, this paste requires a more significant amount of water to obtain equivalent workability.

The T.BA.FA and T.BA.SF samples demonstrated similar behaviour, showing a loss in the consistency of approximately 15 and 17% in relation to the T.REF paste (which has a greater spread). Fly ash and silica fume have opposite physical properties, that is, while fly ash has a high grain size and reduced SSA, silica fume, on the other hand, has a high SSA and reduced particle size. Therefore, it can be seen that the partial replacement of cement with SCM's does not seem to determine the effect of the consistency of the pastes. The addition of barite to the matrices was possibly decisive in obtaining the results in the fresh state, given the physical properties of the mineral that tend to justify the consumption of water from the pastes.

4.2. Paste Properties in the Hardened State

The average apparent density results are illustrated in Figure 3. Notably, the standard deviations presented in all cases were less than 0.02, or even in percentage form, less than 0.5%, providing greater reliability to the results. As the samples age, an increase in the apparent density value obtained is noted. The most significant increase observed in this period was in the T.REF folder, with a 3.13% increase, followed by T.BA.SF (2.88%), T.BA (1.16%), and T.BA.FA (0.24%). It was also possible to observe that the pastes with the addition of barium sulfate, as expected, exceeded the density of the T.REF paste by 6 to 10%, in line with what has been reported by several authors who also used this ore as a filling material in several types of matrices [28-31, 55-60].

The paste with added barite (T.BA) was the matrix that showed the most significant increase (approximately 10%) in the density of the T.REF paste, which may be related to the high density of this mineral. Another relevant aspect to be highlighted is that barium sulfate has proven to be satisfactory in incorporating cementitious matrices, given its proven interaction with Portland cement. This reaction can lead to the generation of new hydrated

products, causing a packing of the matrix with the refinement of pores and a reduction in voids, which, in turn, increases the density and durability of the assembly.

Figure 3: Average apparent densities obtained for each cement paste.

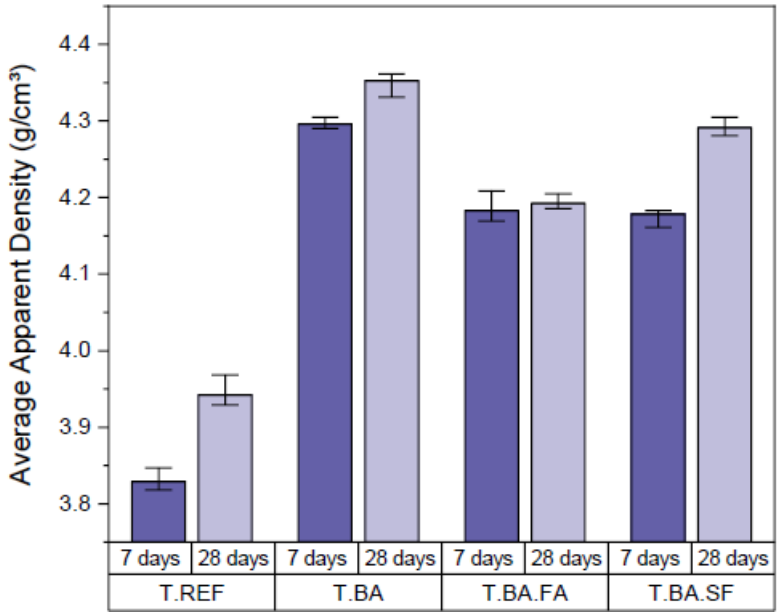

The pastes with partial replacement of Portland cement by SCM's (T.BA.FA and T.BA.SF) showed a decrease in density when compared to the T.BA paste, which is associated with the pozzolanic activity of matrices with the incorporation of SCM's which occurs later. However, even though they showed a reduction (approximately 3.5%), they surpassed the density of the T.REF paste. Therefore, fly ash and active silica as SCM's in cementitious matrices with the incorporation of barium present themselves as a viable option, as also observed by Khalaf, Ban and Ramli [61], Pires *et al.* [28], Eltawil *et al.* [62], Shalbi *et al.* [63], Pires *et al.* [29], Oglat and Shalbi [64] and Abdullah *et al.* [65]. Finally, it is noteworthy that the density of T.BA.FA did not change as the samples aged, while the T.BA.SF paste showed an increase of approximately 3% in the same period.

Figure 4 illustrates the mechanical test results carried out on the pastes, highlighting the reduced standard deviations presented in each result, with the maximum value obtained

in the T.REF paste aged 28 days (1.90). Although mechanical tests may present variations in results due to several external factors (press calibration, sample moulding, curing, among others), no significant deviations were observed. It can also be seen that in all samples, there was a significant evolution in resistance as the breaking age progressed, representing an increase of approximately 146% for the T.BA.FA paste, 151% for T.BA, 164% for T.REF and 272% for the T.BA.SF paste from 7 to 28 days of curing.

Figure 4: Axial compression strengths obtained for each cement paste.

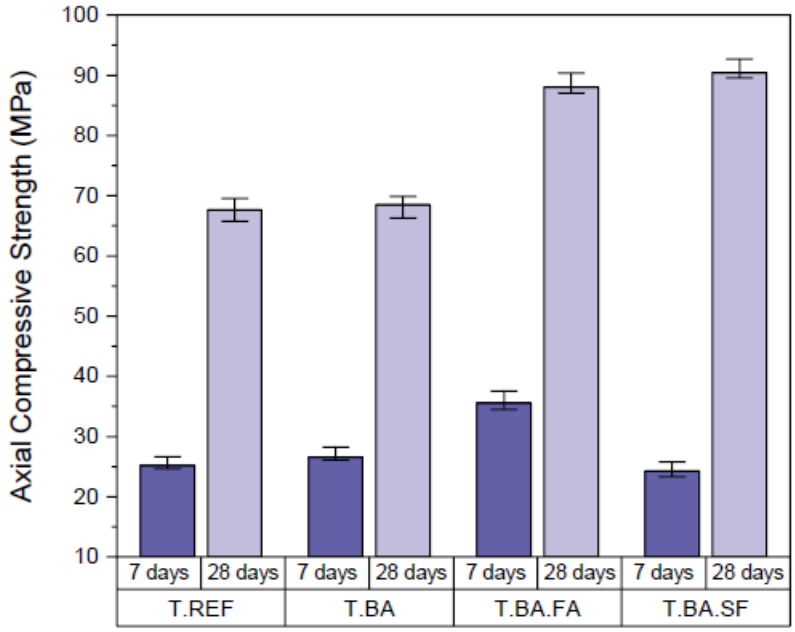

Regarding the resistance values of T.REF and T.BA, at both rupture ages, the results were equivalent, differing by only 6%. Therefore, it is possible to infer that adding barium to the T.BA paste did not negatively influence the development of its mechanical properties. Some authors, such as Horszczaruk and Brzozowski [66] and Bouali *et al.* [67] observed that the addition of barite to cementitious matrices negatively interfered with the development of compressive strength over time (about a reference sample without the addition of ore). However, recent research carried out by Sayyed *et al.* [68], Huang *et al.* [69] and Mansoori, Morshedian and Darounkola [70] validated, in a different way from previous studies, that barium sulfate

participated in the hydration reactions of Portland cement in a positive way, thus favouring the development of the mechanical resistance of the matrices. The study by Kök *et al.* [71] presents relevant data on incorporating this ore. According to the authors, the resistance of cementitious samples with barite increases as the addition of barium sulfate increases, suggesting that the mineral possibly favours the hydration reactions of Portland cement.

Evaluating the pastes with the replacement of Portland cement by fly ash and silica fume (T.BA.FA and T.BA.SF), an increase in resistance of 31 and 34%, respectively, can be seen when compared to the T.REF paste of the same age. The development of the mechanical properties of pastes with SCM's is justified due to the effective hydration process of these matrices. In this chemical reaction, among other hydrated products, C-S-H is generated from the reaction of calcium silicates with water, being the compound responsible for the gain of resistance in cement matrices [72-73]. The formation of this hydrated product may be associated with the physical and chemical aspects of the materials that make up the pastes, in addition to their synergistic reactions at the time of hydration.

Analyzing the physical properties of the materials, it is observed that barium pastes contribute to increasing the SSA of the matrix since the SSA of barium is 110% greater than that of cement. In the case of T.BA.SF, the high SSA of silica about cement (1000% higher), stands out. It is known that grain size significantly contributes to these materials' reactivity and their respective pozzolanic activities [74-75]. Silica fume and barium sulfate, having high SSA, acted as extra nucleation points for forming C-S-H, thus justifying the high resistances achieved [76-78]. Furthermore, as observed in the chemical characterization, fly ash and silica fume have a high supply of pozzolanic oxides that enhance the hydration reactions of the matrix. In this way, there is a more abundant formation of hydrated products, refining the system by reducing free spaces (pores) [79-80]. Therefore, they can justify the high mechanical performance of the T.BA.FA and T.BA.SF pastes.

4.3. Attenuating Properties of Photon Beams

Figure 5 illustrates the percentage of radiation transmitted by each sample, covering all thicknesses investigated in this study, as outlined in the protocol in Section 3.4. Each frame represents one of the four cement pastes studied, named: T.REF, T.BA, T.BA.FA and T.BA.SF. The experiments used photon beams with two voltages, 6 and 10 MV. Each point represents the arithmetic mean of three identical readings measured by the electrometer behind each sample. As the maximum standard deviation obtained in all readings was less than 0.2%, the error bars associated with this quantity were removed from the Figure in order to facilitate the visualization of the data, since they are very small.

Figure 5: Percentage of transmitted radiation depending on the thickness of the samples. The square represents measurements for 6 MV and the triangle for 10 MV. Each table represents one of the four cement pastes studied, called: a) T.REF, b) T.BA, c) T. BA.FA and d) T. BA.SF. Transmission values were normalized by their respective local maxima.

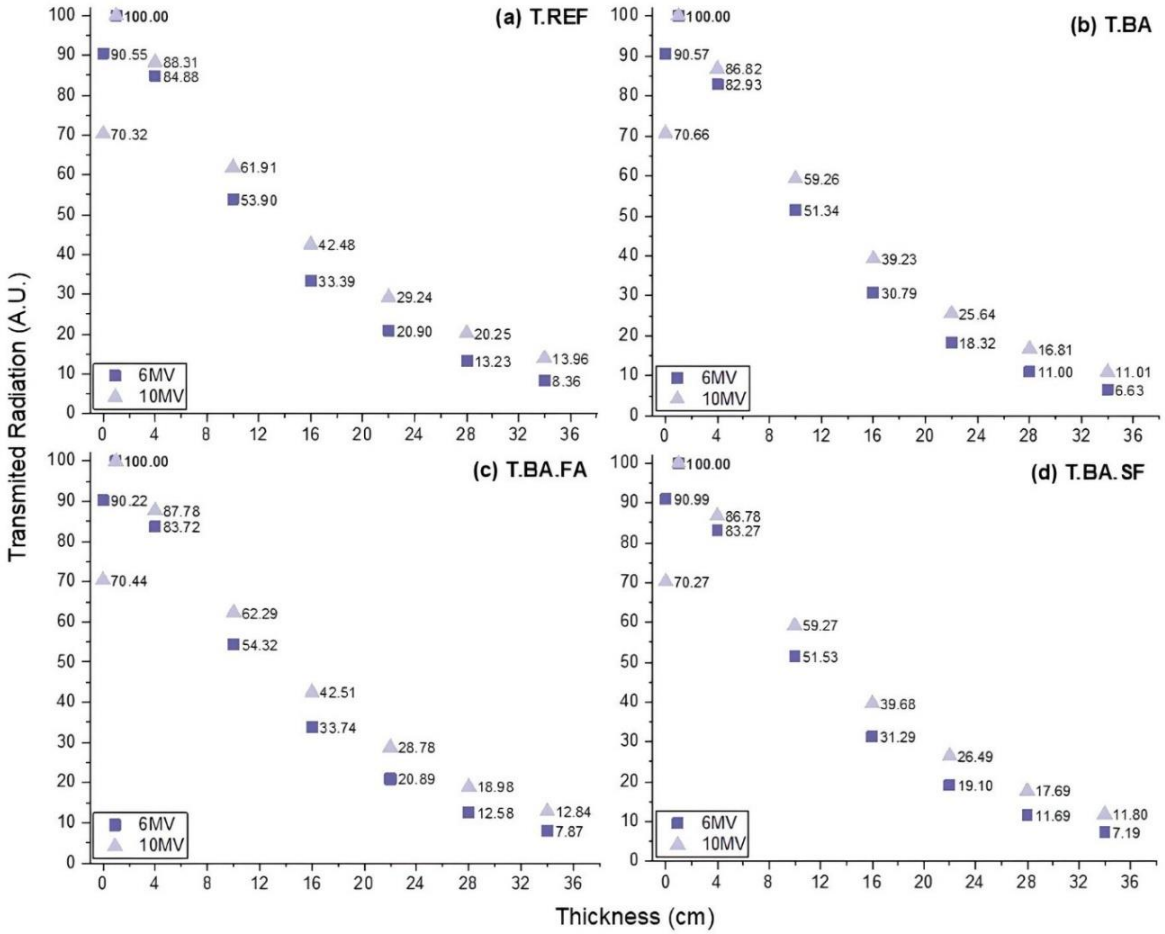

In general, the percentage of transmitted radiation for both voltages decrease exponentially as the thickness of the samples increases, as predicted by the Beer-Lambert Law [81]. However, an initial dose increase for the sample of 1.0 cm can be observed about the direct beam (unshielded). As it is a beam aimed at radiotherapy, unlike diagnostic radiology, energies in the range of hundreds of keV are used, creating build-up regions in the material. This phenomenon occurs due to the lack of electronic balance resulting from the kinetic energy transferred by the incident photon beam to the secondary electrons in the medium. Load balance occurs at the end of the build-up region and corresponds to the point of maximum dose located at approximately 1.0 cm. This position directly depends on the energy of the incident beam and the attenuating material, as seen in Figure 5.

By the determinations imposed by the National Nuclear Energy Commission (CNEN), through CNEN Standard NN 6.10 [82], the values of semi-reductive and de-reductive layers must be referenced during the shielding calculation in the Final Safety Analysis Report. Therefore, the attenuation of the beam was evaluated for a de-reductive layer, corresponding to 90% of the original intensity. Thus, the results of the thicknesses required to meet international standards, as well as the linear attenuation coefficients, maximum intensities and determination coefficients are presented in Table 8. Therefore, evaluating the values obtained for the de-reductive layer, it was possible to verify that the samples with barite provided a reduction in the barrier thickness of approximately 10% when compared to the reference sample.

However, although the calculation of the barrier thickness for shielding in radiotherapy considers the values of the de-reductive layers, a comparative analysis of the results of the thicknesses (x) of the samples obtained experimentally at the highest voltage of the electron linear accelerator (10 MV) was performed. Thus, the T.BA.FA and T.BA.SF pastes showed the potential to reduce up to 81% of the thickest wall of the radiotherapy room used to perform the measurements (200.0 cm) in addition to maintaining the transmitted radiation at

recommended levels (<10%). This finding, although promising, requires further investigation to return significant conclusions about cost reductions and architectural projections of these environments meeting the radiotherapy dimensioning criteria.

The results indicate that all pastes require a thickness lower than the T.REF reference for shielding the photon beam, with emphasis on the mixture containing only barite (T.BA), which presents a decrease in thickness of 3.04 cm for 6 MV and 5.33 cm for 10 MV, about the T.REF reference. Even smaller thicknesses can be achieved by increasing the proportion of barite in the mixture, however, due to the complexity, this aspect constitutes a research topic for future studies. From the point of view of pastes incorporating SCM's, it was observed that the T.BA.SF composition provided superior shielding effectiveness compared to the T.BA.FA composition. This finding is supported by the presentation of a higher average apparent density as evidenced in Figure 3.

Table 8: Adjustment parameters used in exponential regression for each of the cement pastes, in which: (x) thickness necessary to attenuate 90% of the maximum radiation intensity, (k) linear attenuation coefficient, (I_0) maximum intensity and, (R^2) determination coefficient.

VOLTAGES /	**6 MV**				**10 MV**			
CEMENT PASTE	x (cm)	k (1/cm)	I_0 (%)	R^2 (%)	x (cm)	k (1/cm)	I_0 (%)	R^2 (%)
T.REF	31.11	0.074	105.30	97.40	37.74	0.061	110.60	99.73
T.BA	28.78	0.080	106.30	97.39	33.86	0.068	112.70	99.65
T.BA.FA	30.70	0.075	106.10	97.31	36.54	0.063	112.60	99.58
T.BA.SF	29.52	0.078	105.60	97.61	34.88	0.066	111.30	99.75

5. DISCUSSIONS

The results obtained were related to identifying which properties were decisive for the performance of the pastes against ionizing radiation shielding. Figure 6a illustrates the consistency results related to the apparent density (at 28 days) for all pastes evaluated in this study. A behavioural trend can be seen, the higher the density of the pastes, the lower the spread obtained. The T.BA paste had the highest density and the lowest average spread. This

relationship is associated with the physical and morphological properties of the materials that make up the matrix, which, consequently, directly influence the water consumption of the sample. This relationship between consistency and density was observed linearly in all samples, evidenced by the trend line's high coefficient of determination (R^2) (~ 97%).

Figure 6: Relationship of the results of the four pastes evaluated between: a) consistency and apparent density at 28 days of age, b) axial compression strength at 28 days of age and consistency and, c) axial compression strength at 28 days of age.

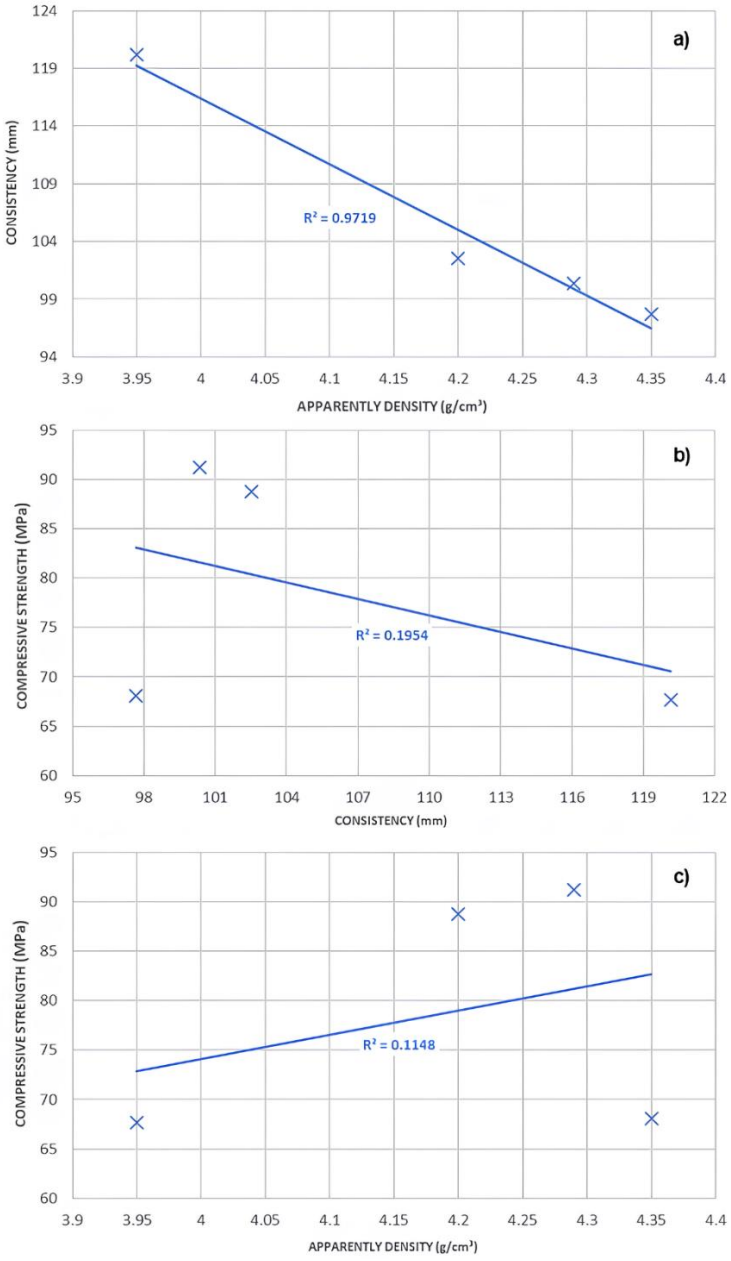

Although the relationship between apparent density and scattering showed a high interaction, they do not correspond when individually related to the results of axial compression resistance at 28 days of age, as can be seen in Figure 6b and Figure 6c. From the trend line drawn in both Figures, it would be possible to infer that there would be greater resistance in smaller spreads, and greater packing densities would provide an evolution in the mechanical properties of the samples, which is expected in Portland cement matrices. However, this cannot be stated due to the reduced relationship between these variables (R^2 < 20%). Although the mechanical test presented a reduced standard deviation with small variance between the results, under the conditions of this research it could not justify or complement the results of apparent density, nor consistency.

Figure 7a illustrates the results of axial compression resistance at 28 days of age, related to the radiation transmitted to a 34.0 cm specimen for the two voltages of the linear electron accelerator. In this way, it is clear that the mechanical properties of the pastes, in addition to not justifying the results of consistency and apparent density, are also not related to the results of attenuation of photon beams. Although this study is also dedicated to analyzing the mechanical properties of Portland cement matrices, this characteristic is not predominant for understanding the behaviour of new materials when shielding ionizing radiation.

Adversely, it is possible to see in Figure 7b and Figure 7c the consistency and apparent density results of the 28-day-old pastes, also related to the radiation transmitted by a 34.0 cm block for the same linear accelerator voltages. These two properties (consistency and density) are relevant for the study and analysis of new materials used in photon beam protection barriers. As the spreading of the pastes in the fresh state increases, the radiation transmitted by the sample also increases for the two analysis voltages, that is, the greater the amount of free water in the matrix, the lower its attenuating performance. In summary, this result may indicate two behavioural trends for

synthesising new barrier materials with satisfactory results: I) adopting lower w/s ratios or, II) using materials requiring more water in the mixture.

Figure 7: Relationship between the radiation transmitted at 6 and 10 MV for the sample with 34.0 cm for the four pastes evaluated and: a) resistance to axial compression at 28 days of age, b) consistency and, c) apparent density at 28 days of age.

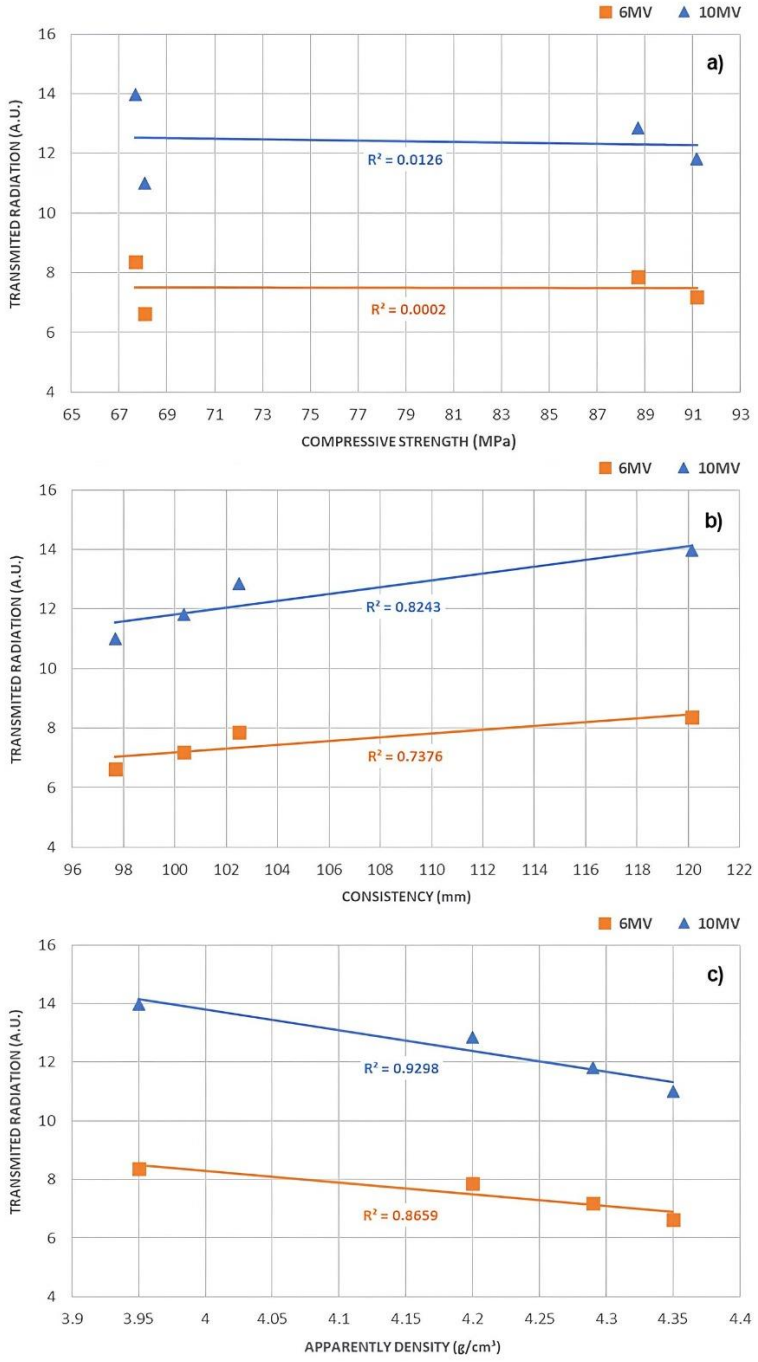

About the apparent density, as expected, the higher the result obtained for the pastes under analysis, the lower the percentage of radiation transmitted by the 34.0 cm block both at 6 MV and 10 MV. It is already known that radiation attenuation properties are closely related to the density of the absorbing material [7- 8], and this trend is observed graphically with the results illustrated in Figure 7c. It is also worth highlighting the significant coefficients of determination obtained (87 and 93%), especially at the 10 MV (highest analysis voltage), possibly justifying this trend of increasing the density of the absorbing material versus reducing the radiation transmitted by it.

6. CONCLUSIONS

This study investigated the properties of Portland cement pastes in shielding photon beams from a linear electron accelerator in a radiotherapy room. To this end, the response factors analyzed together provided the following conclusions:

a) The addition of barium sulfate to the matrices directly influenced the properties of the fresh state, which requires greater water consumption due to the physical properties of barium (high SSA and reduced grain size);

b) Regarding the properties in the hardened state, especially the apparent density of the pastes, it was observed that adding barite significantly improved the results for all pastes at 7 and 28 days. This aspect is justified due to the high specific mass of barium which, in this case, was 42%, 90% and 104% greater than the specific mass of Portland cement, silica fume and fly ash, respectively. Furthermore, the incorporation of barium in the mixtures may have favored the hydration reactions, considering that the T.BA paste presented results equivalent to the T.REF paste, however, with a slight tendency to increase at the two breaking ages. In the case of pastes with partial replacement of Portland cement by SCM's, there was a significant evolution of mechanical

resistance with the development of ages since barium sulfate may have contributed significantly to both the pozzolanic activity of fly ash and silica fume;

c) In the analysis of the properties of the pastes regarding shielding of ionizing radiation, it was proven that the addition of barite improved the attenuation performance of the samples at the two voltages evaluated (6 and 10 MV). The pastes with partial replacement of Portland cement by SCMs presented reduced shielding when compared to T.BA, with the sample with silica fume being more attenuating than the one with fly ash. This result becomes relevant, since the pastes presented excellent mechanical properties and shielding effectiveness, proving to be an environmentally sustainable option. That said, they provide a reduction in the consumption of Portland cement and, consequently, enable reductions in the emissions of pollutant gases (CO_2) from the manufacturing process of clinker (main compound of Portland cement). Finally, it was possible to infer that T.BA is capable of reducing the thickness of the protective barrier by up to 10% when compared to T.REF for a voltage of 10 MV;

d) After listing the results obtained, it was found that only one property evaluated was relevant to understanding the study. Although mechanical resistance is a relevant property of the structural aspect for the design of new environments, within the scope of this study, when related to shielding results, it presented $R^2 < 1.3\%$. On the other hand, the apparent density results when related to shielding, presented R^2 of approximately 87% at 6 MV and 93% at 10 MV, thus indicating that in the design of new materials acting on shielding, this property tends to be the more relevant.

ACKNOWLEDGMENT

The authors extend their thanks to the Coordination for the Improvement of Higher Education Personnel (CAPES), the National Council for Scientific and Technological Development (CNPq), the Santa Casa de Misericórdia of Porto Alegre (Rio Grande do Sul/Brazil), the Laboratory of Characterization of Materials Valorization (LCVMat) and the Construction Materials Laboratory (LMC) at Universidade do Vale do Rio dos Sinos (UNISINOS).

FUNDING

This study was financed in part by the Coordenação de Aperfeiçoamento de Pessoal de Nível Superior – Brasil (CAPES) – Finance Code 001.

CONFLICT OF INTEREST

The authors declare no conflict of interest.

REFERENCES

[1] Chandra R A, Keane F K, Voncken F E, Thomas C R. Contemporary radiotherapy: present and future. **The Lancet**, v.398, n. 10295, p.171-184, 2021. https://doi.org/10.1016/S01406736(21)00233-6.

[2] Guan H, Zhou Z, Hou X, Zhang F, Zhao J, Hu K. Safety and potential increased risk of toxicity of radiotherapy combined immunotherapy strategy. **Asia-Pacific Journal of Clinical Oncology**, v. 19, n. 1, p. 35-50, 2023. https://doi.org/10.1111/ajco.13688.

[3] Barton M B, Jacob S, Shafiq J, Wong K, Thompson S R, Hanna T P, *et al.* Estimating the demand for radiotherapy from the evidence: a review of changes from 2003 to 2012.

Radiotherapy and oncology, v. 112, n. 1, p. 140-144, 2014. https://doi.org/10.1016/j.radonc.2014.03.024.

[4] Chandra R A, Kachnic L A, Thomas JR C R. Contemporary topics in radiation medicine, part I: current issues and techniques. **Elsevier Health Sciences**, v. 33, n. 6, 2019. https://doi.org/10.1016/S0889-8588(19)30132-7.

[5] Chandra R A, Kachnic L A, Thomas JR C R. Contemporary topics in radiation medicine, part II: disease sites. **Hematol Oncol Clinics**, v. 34, n. 10.1016, p. S0889-8588, 2020. https://doi.org/10.1016/S0889-8588(19)30145-5.

[6] De Ruysscher D, Niedermann G, Burnet N G, Siva S, Lee A W, *et al.* Radiotherapy toxicity. **Nature Reviews Disease Primers**, v. 5, n. 1, p. 13, 2019. https://doi.org/10.1038/s41572-019-0064-5.

[7] Campbell G S, Norman J. An introduction to environmental biophysics. **Berlin: Springer Science & Business Media**; 2012. https://doi.org/10.1007/978-1-4612-1626-1.

[8] Scaff L A M. Física na radioterapia: a base analógica de uma era digital. São Paulo: Projeto Saber; 2000. ISBN-10: 8598626112.

[9] Nouailhetas Y. Apostila Educativa: Radiações ionizantes e a vida. Rio de Janeiro: Comissão Nacional de Engenharia Nuclear; 2012. Available at: https://www.gov.br/cnen/pt-br/material-divulgacao-videos-imagens-publicacoes/publicacoes-1/radiacoesionizantes.pdf. Accessed on: 27 Jul. 2023.

[10] Gbetchedji A A, Mansouri I, Hounsossou H C, Houndetoungan G D, Gbaguidi B A, Haddy N, *et al.* Experimental Assessment of Workplace Radiation Exposure in Diagnostic X-ray Medical Imaging Centres in Benin from 2019 to 2020. **Annals of Work Exposures and Health**, v. 65, n. 8, p. 988-997, 2021. https://doi.org/10.1093/annweh/wxab046.

[11] Huhn A, Vargas M, Melo J, Gelbcke F L, Ferreira M L, Lança L. Implementation of a radiation protection program: opinion of the health team working in a radiology service. **Texto & Contexto-Enfermagem**, v. 26, p. e5370015, 2017. https://doi.org/10.1590/0104-07072017005370015.

[12] Cuttler J M. Application of low doses of ionizing radiation in medical therapies. **Dose-response**, v. 18, n. 1, p. 1559325819895739, 2020. https://doi.org/10.1177/1559325819895739.

[13] Thellier S, Poret C, Carminati S. Radiotherapy risk management: Going beyond the concept of safety barriers. **Radioprotection**, v. 56, n. 3, p. 211-219, 2021. https://doi.org/10.1051/radiopro/2021021.

[14] Agrawal V, Paulose R, Arya R, Rajak G, Giri A, Bijanu A, *et al.* Green conversion of hazardous red mud into diagnostic X-ray shielding tiles **Journal of Hazardous Materials**, v. 424, p. 127507, 2022. https://doi.org/10.1016/j.jhazmat.2021.127507.

[15] Sarker D, Biswas A, Rahman M, Mehedi M. Optimization of radiation shielding concrete for radiotherapy treatment room at Bangabandhu sheikh mujib medical university. **Key Engineering Materials**, v. 705, p. 338-344, 2016. https://doi.org/10.4028/www.scientific.net/KEM.705.338.

[16] Amritphale S S, Anshul A, Chandra N, Ramakrishnan N. A novel process for making radiopaque materials using bauxite-Red mud. **Journal of the European Ceramic Society**, v. 27, n. 4, p. 1945-1951, 2007. https://doi.org/10.1016/j.jeurceramsoc.2006.05.106.

[17] Chauhan R K, Mudgal M, Verma S, Amritphale S S, Das S, Shrivastva A. Development and design mix of radiation shielding concrete for gamma-ray shielding. **Journal of Inorganic and Organometallic Polymers and Materials**, v. 27, p. 871-882, 2017. https://doi.org/10.1007/s10904-017-0531-y.

[18] Zayed A M, Masoud M A, Rashad A M, El-Khayatt A M, Sakr K, Kansouh W A, *et al.* Influence of heavyweight aggregates on the physico-mechanical and radiation attenuation properties of serpentine-based concrete. **Construction and Building Materials**, v. 260, p. 120473, 2020. https://doi.org/10.1016/j.conbuildmat.2020.120473.

[19] Arfa M M, Sadawy M M, Nooman M T, Farag A T M, El Shazly R M. The influence of heating on mechanical and nuclear properties of reactive powder concrete as a protective shield in nuclear facilities. **Progress in Nuclear Energy**, v. 143, p. 104046, 2022. https://doi.org/10.1016/j.pnucene.2021.104046.

[20] Sadeq M S, Bashter I I, Salem S M, Mansour S F, Saudi H A, Sayyed M I, *et al.* Enhancing the gamma-ray attenuation parameters of mixed bismuth/barium borosilicate glasses: using an experimental method, Geant4 code and XCOM software. **Progress in Nuclear Energy**, v. 145, p. 104124, 2022. https://doi.org/10.1016/j.pnucene.2022.104124.

[21] AbuAlRoos N J, Amin N A B, Zainon R. Conventional and new lead-free radiation shielding materials for radiation protection in nuclear medicine: A review. **Radiation**

Physics and Chemistry, v. 165, p. 108439, 2019.https://doi.org/10.1016/j.radphyschem.2019.108439.

[22] Alorfi H S, Hussein M A, Tijani S A. The use of rocks in lieu of bricks and concrete as radiation shielding barriers at low gamma and nuclear medicine energies. **Construction and Building Materials**, v. 251, p. 118908, 2020. https://doi.org/10.1016/j.conbuildmat.2020.118908.

[23] Sharma A, Sayyed M I, Agar O, Kaçal M R, Polat H, Akman F. Photon-shielding performance of bismuth oxychloride-filled polyester concretes. **Materials Chemistry and Physics**, v. 241, p. 122330, 2020. https://doi.org/10.1016/j.matchemphys.2019.122330.

[24] Li Z, Zhou W, Zhang X, Gao Y, Guo S. High-efficiency, flexibility and lead-free X-ray shielding multilayered polymer composites: Layered structure design and shielding mechanism. **Scientific reports**, v. 11, n. 1, p. 4384, 2021. https://doi.org/10.1038/s41598-021-83031-4.

[25] Ahmed R, Saad Hassan G, Scott T, Bakr M. Assessment of Five Concrete Types as Candidate Shielding Materials for a Compact Radiation Source Based on the IECF. **Materials**, v. 16, n. 7, p. 2845, 2023. https://doi.org/10.3390/ma16072845.

[26] Turhan M F, Akman F, Kaçal M R, Polat H, Demirkol İ. A study for gamma-ray attenuation performances of barite filled polymer composites. **Applied Radiation and Isotopes**, v. 191, p. 110568, 2023. https://doi.org/10.1016/j.apradiso.2022.110568.

[27] El-Samrah M G, Abdel-Rahman M A, El Shazly R M. Effect of heating on physical, mechanical, and nuclear radiation shielding properties of modified concrete mixes. **Radiation Physics and Chemistry**, v. 153, p. 104-110, 2018. https://doi.org/10.1016/j.radphyschem.2018.09.018.

[28] Pires M M, Nascimento C D, Souza E G, Kruger K, Hoff G. Utilização de sulfato de bário como constituinte de concreto para blindagem de salas de radiologia. **Matéria (Rio de Janeiro)**, v. 26, n. 04, p. e13103, 2021. https://doi.org/10.1590/S1517-707620210004.1303.

[29] Pires M M, Nascimento C D, Souza E G, Hoff G, Kulakowski M P. Estudo de blindagem para salas de radioterapia: uma aplicação para concretos baritados. **Matéria (Rio de Janeiro)**, v. 27, p. e202248962, 2022. https://doi.org/10.1590/1517-7076-RMAT-2022-48962.

[30] Yin S, Wang H, Li A, Ma Z, He Y. Study on Radiation Shielding Properties of New Barium-Doped Zinc Tellurite Glass. **Materials**, v. 15, n. 6, p. 2117, 2022. https://doi.org/10.3390/ma15062117.

[31] Amin M N, Ahmad I, Iqbal M, Abbas A, Khan K, Faraz M I, *et al.* Computational AI models for investigating the radiation shielding potential of high-density concrete. **Materials**, v. 15, n. 13, p. 4573, 2022. https://doi.org/10.3390/ma15134573.

[32] Tochaikul G, Mongkolsuk M, Kobutree P, Kawvised S, Pairodsantikul P, Wongsa P, *et al.* Properties of cement Portland composite prepared with Barium sulfate and Bismuth oxide for radiation shielding. **Radiation Effects and Defects in Solids**, v. 179, n. 3-4, p. 548-566, 2024. https://doi.org/10.1080/10420150.2023.2294037.

[33] Zezulová A, Staněk T, Opravil T. The influence of barium sulphate and barium carbonate on the Portland cement. **Procedia Engineering**, v. 151, p. 42-49, 2016. https://doi.org/10.1016/j.proeng.2016.07.358.

[34] Skibsted J, Snellings R. Reactivity of supplementary cementitious materials (SCMs) in cement blends. **Cement and Concrete Research**, v. 124, p. 105799, 2019. https://doi.org/10.1016/j.cemconres.2019.105799.

[35] Snellings R, Suraneni P, Skibsted J. Future and emerging supplementary cementitious materials. **Cement and concrete research**, v. 171, p. 107199, 2023. https://doi.org/10.1016/j.cemconres.2023.107199.

[36] Kharita M H, Takeyeddin M, Alnassar M, Yousef S. Development of special radiation shielding concretes using natural local materials and evaluation of their shielding characteristics. **Progress in Nuclear energy**, v. 50, n. 1, p. 33-36, 2008. https://doi.org/10.1016/j.pnucene.2007.10.004.

[37] Madej D, Silarski M, Parzych S. Design, structure, microstructure and gamma radiation shielding properties of refractory concrete materials containing Ba-and Sr-doped cements. **Materials Chemistry and Physics**, v. 260, p. 124095, 2021. https://doi.org/10.1016/j.matchemphys.2020.124095.

[38] Badarloo B, Lehner P, Bakhtiari Doost R. Mechanical properties and gamma radiation transmission rate of heavyweight concrete containing barite aggregates. **Materials**, v. 15, n. 6, p. 2173, 2022. https://doi.org/10.3390/ma15062173.

[39] El-Samrah M G, Zamora M A, Novog D R, Chidiac S E. Radiation shielding properties of modified concrete mixes and their suitability in dry storage cask.

Progress in Nuclear Energy, v. 148, p. 104195, 2022. https://doi.org/10.1016/j.pnucene.2022.104195.

[40] Al-Ghamdi H, Elsafi M, Sayyed M I, Almuqrin A H, Tamayo P. Performance of newly developed concretes incorporating WO3 and barite as radiation shielding material. **Journal of Materials Research and Technology**, v. 19, p. 4103-4114, 2022. https://doi.org/10.1016/j.jmrt.2022.06.145.

[41] Nabil I M, El-Samrah M G, Omar A, Tawfic A F, El Sayed A F. Experimental, analytical, and simulation studies of modified concrete mix for radiation shielding in a mixed radiation field. **Scientific Reports**, v. 13, n. 1, p. 17637, 2023. https://doi.org/10.1038/s41598-023-44978-8.

[42] Abualroos N J, Yaacob K A, Zainon R. Radiation attenuation effectiveness of polymer-based radiation shielding materials for gamma radiation. **Radiation Physics and Chemistry**, v. 212, p. 111070, 2023. https://doi.org/10.1016/j.radphyschem.2023.111070.

[43] Pires M M, Sobreira L C, Maia I Z, Ribeiro F R C, Rodrigues N M, Souza E G, *et al.* Building construction materials for ionizing radiation shielding: a systematic literature review. **Caderno Pedagógico**, v. 21, n. 1, p. 3129-3162, 2024. https://doi.org/10.54033/cadpedv21n1-168.

[44] Berodier E, Scrivener K. Understanding the Filler Effect on the Nucleation and Growth of C-S-H. **Journal of the American Ceramic Society**, v. 97, n. 12, p. 3764-3773, 2014. https://doi.org/10.1111/jace.13177.

[45] Scrivener K, Snellings R, Lothenbach B. A practical guide to microstructural analysis of cementitious materials. Boca Raton: Taylor & Francis Group; 2016. ISBN-13: 978-1-4987-3867-5.

[46] Mantellato S, Palacios M, Flatt R J. Impact of sample preparation on the specific surface area of synthetic ettringite. **Cement and Concrete Research**, v. 86, p. 20-28, 2016. https://doi.org/10.1016/j.cemconres.2016.04.005.

[47] Brazilian Association of Technical Standards. ABNT NBR 5738:2015: Concrete - Procedure for molding and curing concrete test specimens. Rio de Janeiro: ABNT; 2015.

[48] Kantro D L. Influence of water-reducing admixtures on properties of cement paste - a miniature slump test. **Cement, Concrete, and Aggregates**, v. 2, n. 2, p. 95-102, 1980. https://doi.org/10.1520/CCA10190J.

[49] Brazilian Association of Technical Standards. ABNT NBR 7215:2019: Portland cement - Determination of compressive strength of cylindrical test specimens. Rio de Janeiro: ABNT; 2019.

[50] Mehdipour I, Khayat K H. Elucidating how particle packing controls rheology and strength development of dense cementitious suspensions. **Cement and Concrete Composites**, v. 104, p. 103413, 2019. https://doi.org/10.1016/j.cemconcomp.2019.103413.

[51] Campos H F, Rocha T M S, Reus G C, Klein N S, Marques Filho J. Determinação do teor ótimo de substituição do cimento Portland por pó de pedra usando métodos de empacotamento de partículas e análise do excesso de água na consistência de pastas. **Revista IBRACON de Estruturas e Materiais**, v. 12, p. 210-232, 2019. https://doi.org/10.1590/S1983-41952019000200002.

[52] Zhang C, Wang A, Tang M, Liu, X. The filling role of pozzolanic material. **Cement and concrete research**, v. 26, n. 6, p. 943-947, 1996. https://doi.org/10.1016/0008-8846(96)00064-6.

[53] Wang A, Zhang C, Sun W. Fly ash effects: I. The morphological effect of fly ash. **Cement and Concrete Research**, v. 33, n. 12, p. 2023-2029, 2003. https://doi.org/10.1016/S0008-8846(03)00217-5.

[54] Mehdipour I, Khayat K H. Effect of Supplementary Cementitious Material Content and Binder Dispersion on Packing Density and Compressive Strength of Sustainable Cement Paste. **ACI Materials Journal**, v. 113, n. 3, 2016. https://doi.org/10.14359/51688704.

[55] Gökçe H S, Yalçınkaya Ç, Tuyan, M. Optimization of reactive powder concrete by means of barite aggregate for both neutrons and gamma rays. **Construction and building materials**, v. 189, p. 470-477, 2018. https://doi.org/10.1016/j.conbuildmat.2018.09.022.

[56] Mahmoud K A, Sayyed M I, Tashlykov O L. Comparative studies between the shielding parameters of concretes with different additive aggregates using MCNP-5 simulation code. **Radiation Physics and Chemistry**, v. 165, p. 108426, 2019. https://doi.org/10.1016/j.radphyschem.2019.108426.

[57] Azreen N M, Rashid R S, Amran Y M, Voo Y L, Haniza M, Hairie M, *et al.* Simulation of ultra-high-performance concrete mixed with hematite and barite aggregates using Monte Carlo for dry cask storage. **Construction and Building Materials**, v. 263, p. 120161, 2020. https://doi.org/10.1016/j.conbuildmat.2020.120161.

[58] Demir I, Gümüş M, Gökçe, H. S. Gamma ray and neutron shielding characteristics of polypropylene fiber-reinforced heavyweight concrete exposed to high temperatures. **Construction and Building Materials**, v. 257, p. 119596, 2020. https://doi.org/10.1016/j.conbuildmat.2020.119596.

[59] Gharissah M S, Ardiansyah A, Pauziah S R, Muhammad N A, Rahmat R, Heryanto H, *et al.* Composites cement/$BaSO_4$/Fe_3O_4/CuO for improving X-ray absorption characteristics and structural properties. **Scientific Reports**, v. 12, n. 1, p. 19169, 2022. https://doi.org/10.1038/s41598-022-23908-0.

[60] Souza E G, Kruger K, Nascimento C D, Aguzzoli C, Hoff G, Moraes A C B, *et al.* Development of Lead-Free Radiation Shielding Material Utilizing Barium Sulfate and Magnesium Oxide as Fillers in Addition Cure Liquid Silicone Rubber. **Polymers**, v. 15, n. 22, p. 4382, 2023. https://doi.org/10.3390/polym15224382.

[61] Khalaf M A, Ban C C, Ramli M. The constituents, properties and application of heavyweight concrete: A review. **Construction and building materials**, v. 215, p. 73-89, 2019. https://doi.org/10.1016/j.conbuildmat.2019.04.146.

[62] Eltawil K A, Mahdy M G, Youssf O, Tahwia A M. Producing heavyweight high-performance concrete by using black sand as newly shielding construction material. **Materials**, v. 14, n. 18, p. 5353, 2021. https://doi.org/10.3390/ma14185353.

[63] Shalbi S M, Al-Jarrah A M, Jaafar M S, Ahmed N M. Photon Attenuation Coefficients of Fly-Ash Based Geopolymers Synthesized with Different Barite Proportions. **European Journal of Applied Physics**, v. 3, n. 4, p. 1-5, 2021. https://doi.org/10.24018/ejphysics.2021.3.4.84.

[64] Oglat A A, Shalbi S M. An alternative radiation shielding material based on barium-sulphate ($BaSO_4$) - modified fly ash geopolymers. **Gels**, v. 8, n. 4, p. 227, 2022. https://doi.org/10.3390/gels8040227.

[65] Abdullah M A H, Rashid R S M, Amran M, Hejazii F, Azreen N M, Fediuk R, *et al.* Recent trends in advanced radiation shielding concrete for construction of facilities: materials and properties. **Polymers**, v. 14, n. 14, p. 2830, 2022. https://doi.org/10.3390/polym14142830.

[66] Horszczaruk E, Brzozowski P. Investigation of gamma ray shielding efficiency and physicomechanical performances of heavyweight concrete subjected to high temperature. **Construction and Building Materials**, v. 195, p. 574-582, 2019. https://doi.org/10.1016/j.conbuildmat.2018.09.113.

[67] Bouali E, Ayadi A, Kadri E H, Kaci A, Soualhi H, Kallel A. Rheological and mechanical properties of heavy density concrete including barite powder. **Arabian Journal for Science and Engineering**, v. 45, p. 3999-4011, 2020. https://doi.org/10.1007/s13369-019-04331-6.

[68] Sayyed M I, Elsafi M, Almuqrin A H, Cornish K, Elkhatib A M. Novel Shielding Mortars for Radiation Source Transportation and Storage. **Sustainability**, v. 14, n. 3, p. 1248, 2022. https://doi.org/10.3390/su14031248.

[69] Huang X, Xin C, Li J S, Wang P, Liao S, Poon C S, *et al.* Using hazardous barium slag as a novel admixture for alkali activated slag cement. **Cement and Concrete Composites**, v. 125, p. 104332, 2022. https://doi.org/10.1016/j.cemconcomp.2021.104332.

[70] Mansoori E, Morshedian J, Darounkola M R R. Elaboration of X-ray shielding of highly barite-loaded polyester concrete: structure, mechanical properties, and MCNP simulation. **Construction and Building Materials**, v. 370, p. 130650, 2023. https://doi.org/10.1016/j.conbuildmat.2023.130650.

[71] Kök S, Türetken M S, Öksüzer N, Gökçe, H S. Effect of elevated temperature on radiation shielding properties of cement and geopolymer mortars including barite aggregate and colemanite powder. **Materialia**, v. 27, p. 101693, 2023. https://doi.org/10.1016/j.mtla.2023.101693.

[72] Gartner E, Maruyama I, Chen, J. A new model for the CSH phase formed during the hydration of Portland cements. **Cement and Concrete Research**, v. 97, p. 95-106, 2017. https://doi.org/10.1016/j.cemconres.2017.03.001.

[73] Mehta P K, Monteiro P J M. Concreto: Microestrutura, Propriedades e Materiais. São Paulo: Ibracon; 2014. ISBN: 978-85-98576-21-3.

[74] Akcay B, Tasdemir M. Autogenous shrinkage, pozzolanic activity and mechanical properties of metakaolin blended cementitious materials. **KSCE Journal of Civil Engineering**, v. 23, p. 4727-4734, 2019. https://doi.org/10.1007/s12205-019-2401-3.

[75] Liu Y, Lei S, Lin M, Xia Z, Pei Z, Li B. Influence of calcined coal-series kaolin fineness on properties of cement paste and mortar. **Construction and Building Materials**, v. 171, p. 558-565, 2018. https://doi.org/10.1016/j.conbuildmat.2018.03.117.

[76] Scrivener K, Juilland P, Monteiro P. Advances in understanding hydration of Portland cement. **Cement and Concrete Research**, v. 78, p. 38-56, 2015. https://doi.org/10.1016/j.cemconres.2015.05.025.

[77] L'Hôpital E, Lothenbach B, Le Saout G, Kulik D, Scrivener K. Incorporation of aluminium in calcium-silicate-hydrates. **Cement and Concrete Research**, v. 75, p. 91-103, 2015. https://doi.org/10.1016/j.cemconres.2015.04.007.

[78] Wang Y, Shui Z, Gao X, Huang Y, Yu R, Li X, Yang R. Utilizing coral waste and metakaolin to produce eco-friendly marine mortar: Hydration, mechanical properties and durability. **Journal of Cleaner Production**, v. 219, p. 763-774, 2019. https://doi.org/10.1016/j.jclepro.2019.02.147.

[79] Li D, Wei R, Li L, Guan X, Mi X. Pitting corrosion of reinforcing steel bars in chloride contaminated concrete. **Construction and Building Materials**, v. 199, p. 359-368, 2019. https://doi.org/10.1016/j.conbuildmat.2018.12.003.

[80] Zunino F, Martirena F, Scrivener K. Limestone Calcined Clay Cements (LC^3). **ACI Materials Journal**, v. 118, n. 3, 2021. https://doi.org/10.14359/51730422.

[81] Fox M. Optical Properties of Solids (2º ed). Oxford: Oxford University Press; 2010. ISBN-10: 0199573360.

[82] National Nuclear Energy Commission. CNEN NN 6.10: Safety and radiological protection requirements for radiotherapy services. Rio de Janeiro: CNEN; 2017.

LICENSE